

Chiral Modes at Exceptional Points in Exciton-Polariton Quantum FluidsT. Gao,¹ G. Li,² E. Estrecho,^{1,3} T. C. H. Liew,⁴ D. Comber-Todd,¹ A. Nalitov,² M. Steger,⁵ K. West,⁶ L. Pfeiffer,⁶ D. W. Snoke,⁵ A. V. Kavokin,^{2,7,8} A. G. Truscott,⁹ and E. A. Ostrovskaya^{1,3}¹*Nonlinear Physics Centre, Research School of Physics and Engineering, The Australian National University, Canberra, Australian Capital Territory 2601, Australia*²*School of Physics and Astronomy, University of Southampton, SO17 1BJ Southampton, United Kingdom*³*ARC Centre of Excellence in Future Low-Energy Electronics Technologies*⁴*Division of Physics and Applied Physics, School of Physical and Mathematical Sciences, Nanyang Technological University, 21 Nanyang Link, Singapore 637371*⁵*Department of Physics and Astronomy, University of Pittsburgh, Pittsburgh, Pennsylvania 15260, USA*⁶*Department of Electrical Engineering, Princeton University, Princeton, New Jersey 08544, USA*⁷*SPIN-CNR, Viale del Politecnico 1, I-00133 Rome, Italy*⁸*Spin Optics Laboratory, St-Petersburg State University, 1 Ulianovskaya St., St-Petersburg 198504, Russia*⁹*Laser Physics Centre, Research School of Physics and Engineering, The Australian National University, Canberra, Australian Capital Territory 2601, Australia*

(Received 2 June 2017; published 9 February 2018)

We demonstrate the generation of chiral modes—vortex flows with fixed handedness in exciton-polariton quantum fluids. The chiral modes arise in the vicinity of exceptional points (non-Hermitian spectral degeneracies) in an optically induced resonator for exciton polaritons. In particular, a vortex is generated by driving two dipole modes of the non-Hermitian ring resonator into degeneracy. Transition through the exceptional point in the space of the system's parameters is enabled by precise manipulation of real and imaginary parts of the closed-wall potential forming the resonator. As the system is driven to the vicinity of the exceptional point, we observe the formation of a vortex state with a fixed orbital angular momentum (topological charge). This method can be extended to generate higher-order orbital angular momentum states through coalescence of multiple non-Hermitian spectral degeneracies. Our Letter demonstrates the possibility of exploiting nontrivial and counterintuitive properties of waves near exceptional points in macroscopic quantum systems.

DOI: [10.1103/PhysRevLett.120.065301](https://doi.org/10.1103/PhysRevLett.120.065301)

Introduction.—Exceptional points (EPs) in wave resonators of different origins arise when both spectral positions and linewidths of two resonances coincide and the corresponding spatial modes coalesce into one [1,2]. Originally identified as an inherent property of non-Hermitian quantum systems [3–5], EPs have become a focus of intense research in classical systems with gain and loss [6], such as optical cavities [7], microwave resonators [8,9], and plasmonic nanostructures [10]. The counterintuitive behavior of waves in the vicinity of an EP leads to a range of peculiar phenomena, including enhanced loss-assisted lasing [11,12], unidirectional transmission of signals [13], and loss-induced transparency [14].

Because of the nontrivial topology of the EP, the two eigenstates coalesce with a phase difference of $\pm\pi/2$, which results in a well-defined handedness (chirality) of the surviving eigenstate [15]. This remarkable property was first experimentally demonstrated in a microwave cavity [9] and, very recently, enabled observation of directional lasing in optical microresonators [16,17]. So far, the chirality of

the unique eigenstate at an EP has not been demonstrated in any quantum system.

In this Letter, we demonstrate formation of a chiral state at an EP in a macroscopic quantum system of condensed exciton polaritons. Exciton polaritons are hybrid bosons arising due to strong coupling between excitons and photons in semiconductor microcavities [18,19]. Once sufficient density of exciton polaritons is injected by an optical or electrical pump, the transition to quantum degeneracy occurs, whereby typical signatures of a Bose-Einstein condensate emerge [18–23]. Radiative decay of polaritons results in the need for a continuous pump to maintain the population. This intrinsic open-dissipative nature of exciton-polariton condensates offers a new platform for study of non-Hermitian quantum physics. Several recent experiments have exploited the non-Hermitian nature of exciton-polariton systems [24–27]. Importantly, the existence of EPs and the associated topological Berry phase has been demonstrated in an optically induced resonator (quantum billiard) for coherent exciton-polariton waves [27].

An optically induced exciton-polariton resonator is a closed-wall potential arising due to injection of high-energy excitonic quasiparticles by an off-resonant optical pump and strong repulsive interaction between the excitonic reservoir and the condensate [28]. The size of the resonator is comparable to the de Broglie wavelength of the exciton polaritons, and its geometry is defined by the spatial distribution of the optical pump [29–31]. Observation of the EPs in the spectra of exciton-polariton resonators is enabled by two characteristic features of this system. First, the optically confined exciton polaritons form a multimode condensate; i.e. they can macroscopically occupy several single-particle energy states of the pump-induced effective potential [32]. Second, the potential is non-Hermitian, and both real (energy) and imaginary (linewidth) parts of its complex eigenenergies can be precisely controlled by adjusting parameters of the pump [27]. As a result, two or more eigenstates of the system can be brought to degeneracy.

Here, we create a non-Hermitian trapping potential for exciton polaritons in the form of an asymmetric ring resonator and observe condensation into several trapped modes. By changing the geometry of the pump, and therefore the overlap of the modes with the gain region, we observe the transition from crossing to anticrossing of complex eigenvalues, which signals the existence of an EP. Furthermore, our tapered microcavity “wedge” [33] enables precise control over the ratio of the exciton and photon in the hybrid quasiparticle. We use this additional control parameter to drive the two lowest-lying dipole states of the system to a vicinity of an EP and confirm the formation of a chiral mode—a charge one vortex.

Experiment.—We create exciton polaritons in a GaAs/AlGaAs microcavity similar to that used in Ref. [33]. The details of the experimental setup can be found in the Supplemental Material [34]. By utilizing a digital micromirror device (DMD), we create the pump spot of the asymmetric ring shape shown schematically in Fig. 1. The pump simultaneously populates the system

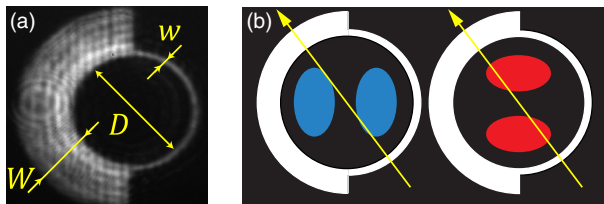


FIG. 1. (a) Experimental pump intensity distribution. The width of the left half-ring is $W = 9 \mu\text{m}$ and is fixed; the width of the right half-ring is tuned between $w_1 = 1.0 \mu\text{m}$ and $w_2 = 1.2 \mu\text{m}$ with a step of $0.1 \mu\text{m}$. The inner ring diameter is $D = 15 \mu\text{m}$ and is fixed. (b) Schematics of the DMD mirror mask shaping the pump spot (white), the direction of the gradient of the cavity wedge (yellow), and the corresponding dipole modes of the trapped exciton polaritons (blue and red).

with exciton polaritons and forms a potential barrier due to the local blue shift in energy induced by the excitonic reservoir [28]. Similar to Ref. [27], the inner area of the ring D is kept constant and the width of one of the potential wall segments w is varied. Analysis of the microcavity photoluminescence by means of energy-resolved near-field (real-space) imaging allows us to obtain the spatial density distribution and energy levels corresponding to the condensate modes in the ring resonator. All experiments are performed in the strong coupling regime, with the pump power approximately 1.5 times above the polariton condensation threshold.

Because of the asymmetry of the potential walls imposed by the pumping geometry and by the cavity wedge [33], the eigenmodes of the optically induced ring resonator resemble the Ince-Gaussian modes [42]. Once the threshold for the condensation is reached, only a few modes are occupied, and we focus on the two dipole modes (1,1) with the orthogonal orientation of the nodal lines. Because of their orientation, the two dipole modes have different overlap with the gain region and are, in general, not energy degenerate and well separated from the other modes (see Supplemental Material [34]).

Because of the non-Hermitian nature of exciton polaritons, the eigenenergy of the modes in the ring potential is also complex, where the real part corresponds to the energy peak position and the imaginary part corresponds to the linewidth. In our experiment, the peak positions corresponding to the two dipole modes can be tuned by changing the relative admixture of exciton and photon in the exciton polariton. This is achieved by keeping all parameters of the pump fixed and changing the relative position between the excitation beam and the sample, as a linear variation in the microcavity width [33] results in variation of detuning between the cavity photon and exciton: $\Delta = E_{\text{ph}} - E_{\text{ex}}$. The change in the energies of the two dipole modes with changing detuning is shown in Fig. 2(a), where a clear crossing of the corresponding energy levels can be observed [43]. The transition to spectral degeneracy is accompanied by an avoided crossing of the imaginary parts of the eigenenergy (linewidths), as seen in Fig. 2(b). Because of the high Q factor of the microcavity (320000) and long lifetime of exciton polaritons (~ 200 ps) [33], the resonances have a very narrow linewidth, which helps to differentiate between closely positioned energy levels.

From the energy-resolved spatial image of the cavity photoluminescence, we reconstruct the spatial probability density distribution of the polariton condensate for each detuning value. Away from the degeneracy, the two dipole modes are clearly visible [Fig. 2(a), insets]. As the two complex eigenvalues are tuned in and out of the degeneracy, we observe the characteristic hybridization and switching of the modes corresponding to the two energy branches. Because of the finite resolution of spectroscopic measurements in our system, it is hard to tune the system

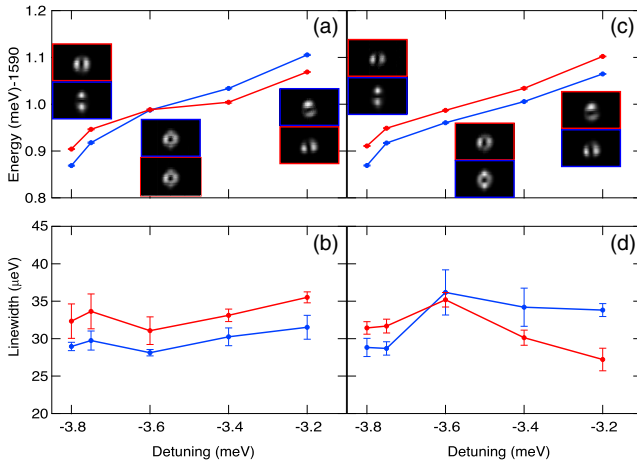


FIG. 2. The (a) crossing of the real parts of the eigenenergies and (b) anticrossing of the imaginary parts of the eigenenergies (linewidths) corresponding to the dipole states for the changing detuning Δ and fixed width of the right half-ring $w_2 = 1.2 \mu\text{m}$. The variation of Δ is produced by moving the excitation beam relative to the sample over the distance of approximately $60 \mu\text{m}$. Insets in (a) show the corresponding spatial density structure of eigenmodes observed in the energy-resolved tomography measurement (see Supplemental Material [34]). The (c) anticrossing of the energies and (d) crossing of the linewidths for the changing detuning Δ and fixed width of the right half-ring $w_1 = 1.0 \mu\text{m}$.

precisely to the EP, whereby both real and imaginary parts of the complex eigenenergy, as well as the eigenstates, would coalesce exactly. To confirm the existence of an EP, we vary the second control parameter, i.e., the width of the right half-ring of the resonator w (see Fig. 1). As its value changes from $w = w_1$ to $w = w_2$, we observe the transition from crossing to anticrossing in energy and from anticrossing to crossing in the linewidths of the two resonances [see Figs. 2(c) and 2(d)]. This transition confirms that an EP exists in the parameter space (Δ, w) [6,27,44]. Furthermore, by fixing the detuning at $\Delta = -3.6 \text{ meV}$, which corresponds to the energy crossing in Fig. 2(a), and tuning w from w_2 to w_1 , we observe a vortexlike mode at $w_1 < w < w_2$, as shown in Fig. 3(e).

In order to establish the nature of this state, we perform interferometry with a magnified ($\times 15$) reference beam derived from a small flat-phase area of the photoluminescence. The energy-resolved interferometric imaging confirms the phase structure of the two dipole modes [Figs. 3(a)–3(d)] away from the degeneracy point. Furthermore, the interference pattern shown in Fig. 3(f) is stable for many minutes and reveals a fork in the fringes, which is a clear signature of a stable charge one vortex. This measurement confirms that a vortex with the topological charge one is formed in the vicinity of the spectral degeneracy, which is only possible if the two dipole modes coalesce with the $\pi/2$ phase difference.

The deterministic nature of the vortex charge is tested in our experiment by blocking the pump for up to 1 h to let the

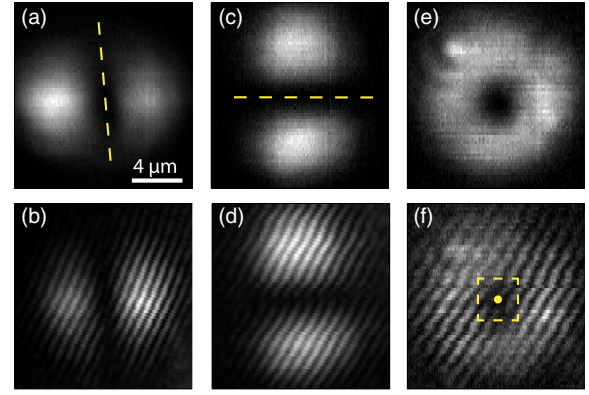


FIG. 3. Experimentally observed (a),(c),(e) probability density distribution of the exciton-polariton condensate and (b),(d),(f) the corresponding interference pattern for the dipole modes with (a),(b) near-vertical and (c),(d) near-horizontal nodal line, and (e),(f) for a charge one vortex state. In (b),(d), the nodal lines can be discerned by the relative shift in fringes. The fork in the fringes marked by the dot in (f) signifies a charge one vortex. Parameters are (a)–(d) $\Delta = -3.8 \text{ meV}$, $w \approx 1.1 \mu\text{m}$; (e),(f) $\Delta = -3.6 \text{ meV}$, $w \approx 1.1 \mu\text{m}$.

pump-injected reservoir disappear. After the pumping is resumed, the sign of the vortex charge remains the same. While the chirality of the mode is assured by the EP, the particular sign of the vortex charge is determined by the orientation of the pump relative to the gradient of the cavity wedge [Fig. 1(b)], which produces a slight chiral asymmetry in the system (see Supplemental Material [34]).

Theory.—The dynamics of an exciton-polariton condensate subject to off-resonant (incoherent) optical pumping can be described by the generalized complex Gross-Pitaevskii equation for the condensate wave function complemented by the rate equation for the density of the excitonic reservoir [45]

$$i\hbar \frac{\partial \psi}{\partial t} = \left[-\frac{\hbar^2}{2m} \nabla^2 + g_c |\psi|^2 + g_R n_R + \frac{i\hbar}{2} (R n_R - \gamma_c) \right] \psi, \\ \frac{\partial n_R}{\partial t} = P(\mathbf{r}) - (\gamma_R + R |\psi|^2) n_R, \quad (1)$$

where $P(\mathbf{r})$ is the rate of injection of reservoir particles per unit area and time determined by the power and spatial profile of the pump, g_c and g_R characterize the interactions between condensed polaritons and between the polaritons and the reservoir, respectively. The decay rates γ_c and γ_R quantify the finite lifetime of condensed polaritons and the excitonic reservoir, respectively. The stimulated scattering rate R characterizes growth of the condensate density.

Assuming that, under cw pumping, the reservoir reaches a steady state, $n_R(\mathbf{r}) = P(\mathbf{r}) / (\gamma_R + R |\psi(\mathbf{r})|^2)$, and that the exciton-polariton density is small near the condensation threshold, Eq. (1) transforms into a linear Schrödinger equation for the condensate confined to an effective non-Hermitian potential [27]

$$V(\mathbf{r}) = V_R(\mathbf{r}) + iV_I(\mathbf{r}) \approx \frac{g_R P(\mathbf{r})}{\gamma_R} + i\frac{\hbar}{2} \left[\frac{RP(\mathbf{r})}{\gamma_R} - \gamma_c \right]. \quad (2)$$

As discussed in the Supplemental Material [34], the dependence on the detuning Δ enters Eq. (1) through the dependence of its parameters on the Hopfield coefficient that characterizes the excitonic fraction of the exciton polariton [18]: $|X|^2 = (1/2)[1 + \Delta/\sqrt{\Delta^2 + E_R^2}]$, where E_R is the Rabi splitting at $\Delta = 0$.

The eigenstates and complex eigenvalues \tilde{E} of the non-Hermitian potential (2) can be found by solving the dimensionless stationary equation

$$[-\nabla^2 + (V' + iV'')]\psi = \tilde{E}\psi, \quad (3)$$

where we have introduced the appropriate scaling [46]. The normalized real $V'(\mathbf{r})$ and imaginary $V''(\mathbf{r})$ parts of the potential depend on detuning via the Hopfield coefficient [46] and are defined by the shape of $P(\mathbf{r})$. For simplicity, we approximate $P(\mathbf{r})$ by Gaussian envelope functions, with the resulting $V'(\mathbf{r})$ and $V''(\mathbf{r})$ shown in Figs. 4(a) and 4(d).

By solving the eigenequation (3) numerically and sorting values of \tilde{E} in the ascending order of their real parts E_n , we obtain the corresponding hierarchy of eigenstates ψ_n . Figures 4(b) and 4(e) show the moduli of ψ_2 and ψ_3 , respectively, which correspond to the slightly deformed dipole states (1,1). The existence of these steady states is also confirmed by full dynamical simulations of Eq. (1) (see Supplemental Material [34]).

The dependence of the real and imaginary parts of the dipole modes' eigenenergies on the experimental control parameters (Δ, w) shown in Fig. 5 confirms that our simple linear model reflects the qualitative behavior observed in the experiment (Fig. 2).

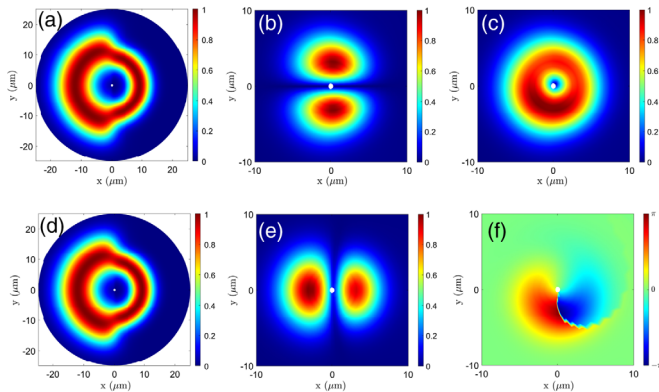


FIG. 4. Approximate complex effective potential and the typical profiles of the dipole modes: (a) $V'(\mathbf{r})$, (d) $V''(\mathbf{r})$, (b) $|\psi_2|$, (c) $|\psi_2 + i\psi_3|$, (e) $|\psi_3|$. (f) The phase distribution corresponding to (c).

To understand why the experimental control parameters Δ and w allow us to tune the system in and out of the vicinity of the EP, we follow the standard approach [2,6,27,49] and construct a phenomenological coupled-mode model for the two modes with the quantum numbers n and n' near degeneracy (see Supplemental Material [34] for details). The effective two-mode Hamiltonian can be written as follows:

$$\hat{H} = \begin{bmatrix} \tilde{E}_n & q \\ q^* & \tilde{E}_{n'} \end{bmatrix}, \quad \tilde{E}_{n,n'} = E_{n,n'} - i\Gamma_{n,n'}, \quad (4)$$

where $\tilde{E}_{n,n'}$ are the complex eigenenergies of the uncoupled modes and q characterizes their coupling strength. The eigenvalues of the Hamiltonian (4) are $\lambda_{n,n'} = \tilde{E} \pm \sqrt{\delta\tilde{E}^2 + |q|^2}$, where $\tilde{E} = (\tilde{E}_n + \tilde{E}_{n'})/2 \equiv E + i\Gamma$, and $\delta\tilde{E} = (\tilde{E}_n - \tilde{E}_{n'})/2 \equiv \delta E - i\delta\Gamma$. The real and imaginary parts of $\lambda_{n,n'}$ form Riemann surfaces with a branch-point singularity in the space of parameters ($\delta E, \delta\Gamma$) [27], as shown in the Supplemental Material [34]. At the EPs, $i\delta\tilde{E}_{EP} = \pm|q|$, the eigenvalues coalesce $\lambda_n = \lambda_{n'}$. The eigenstates also coalesce and form a single chiral state [2,15]. In our system, the two eigenstates corresponding to $n = 2$ and $n' = 3$ are dipole modes, and therefore the chiral state is a vortex with a topological charge one, as shown in Figs. 4(c) and 4(f) and Figs. 3(e) and 3(f).

The two parameters ($\delta E, \delta\Gamma$) can be related to the experimental parameters (Δ, w). As discussed in the Supplemental Material [34], increasing Δ corresponds to increasing δE and moves the system away from the spectral degeneracy, while increasing w corresponds to decreasing $\delta\Gamma$. Therefore, the variables Δ and w allow us to control the

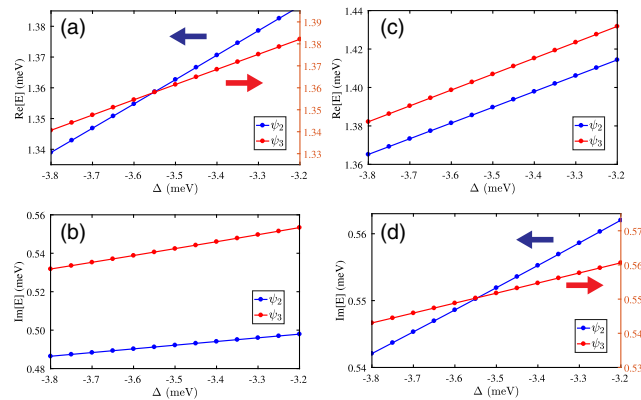


FIG. 5. Behavior of energy levels corresponding to the dipole modes with the change of the exciton-photon detuning Δ . (a) $\text{Re}[\tilde{E}]$ crossing and (b) $\text{Im}[\tilde{E}]$ anticrossing at $w = w_2$. (c) $\text{Re}[\tilde{E}]$ anticrossing and (d) $\text{Im}[\tilde{E}]$ crossing at $w = w_1 < w_2$. (a),(d) Two different y axes accentuate the crossing. The real and imaginary parts of the ground state eigenvalues are subtracted from the absolute values in (a)–(d) [48].

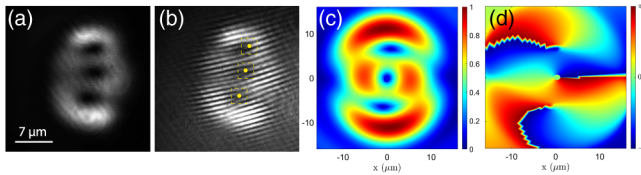


FIG. 6. Experimentally measured (a) density and (b) interference image of the triple-vortex state. Theoretically calculated (c) modulus and (d) phase of the triple-vortex state $\psi = (\psi_7 + i\psi_8) + (\psi_9 + i\psi_{10})$. The three dots in (b) mark the forks in the interference fringes.

approach to the EP as demonstrated in the experiment (Fig. 2) and confirmed by theory (Fig. 5).

Discussion.—In summary, we have experimentally demonstrated the chirality of an eigenstate of a non-Hermitian macroscopic quantum coherent system of Bose-condensed exciton polaritons in the vicinity of an EP. The observed chiral eigenstate is a vortex with a well-defined topological charge (orbital angular momentum), which does not change its sign randomly between realizations of the experiment [50,51]. The controlled generation of a nontrivial orbital angular momentum state protected by the topology of an EP could find use in low-energy polariton-based devices exploiting the non-Hermitian nature of exciton polaritons, in analogy to optical systems with engineered loss and gain [16,17].

The vortices observed here, as well as other quantized vortex flows created spontaneously [52,53] or deliberately [54–56] in the exciton-polariton condensate, are identical to quantum vortices in atomic Bose-Einstein condensates [57–61]. However, the techniques for creating vortices in different quantum fluids are different [62]. Here we present a radically new way of generating a quantum vortex by employing the intrinsic chirality at an EP.

Furthermore, our technique for generating chiral modes can be applied to higher-order orbital angular momentum states. In particular, if the inner size of the ring D is increased, higher-order modes can be populated by the condensate and brought to degeneracy by varying control parameters of the system. Moreover, two (or more) EPs can be simultaneously created and brought to within a close vicinity of each other. As an example, the higher-order orbital momentum state formed in our experiment by hybridization of two chiral modes, $\psi = (\psi_7 + i\psi_8) + (\psi_9 + i\psi_{10})$, is shown in Fig. 6, together with the prediction of our linear theory. The interferometry image confirms that the vortices in the triple-vortex state have the same topological charge (see also a double-vortex state shown in the Supplemental Material [34]). These results open the avenue for experimental studies of EP clustering [63,64] and higher-order EPs [65–69] in a macroscopic quantum system.

This work was partly supported by the Australian Research Council (ARC). T.L. was supported by the Ministry of Education (Singapore) Grant No. 2015-T2-1-055. The work of D. W. S. was supported by the U.S. Army

Research Office Project No. W911NF-15-1-0466. A. V. K. acknowledges the joint Russian-Greek project supported by Ministry of Education and Science of The Russian Federation (project RFMEFI61617X0085). The authors gratefully acknowledge discussions with K. Y. Bliokh.

- [1] M. V. Berry, *Czech. J. Phys.* **54**, 1039 (2004).
- [2] W. D. Heiss, *J. Phys. A* **45**, 444016 (2012).
- [3] C. M. Bender, *Rep. Prog. Phys.* **70**, 947 (2007).
- [4] N. Moiseyev, *Non-Hermitian Quantum Mechanics* (Cambridge University Press, Cambridge, England, 2011).
- [5] I. Rotter and J. P. Bird, *Rep. Prog. Phys.* **78**, 114001 (2015).
- [6] H. Cao and J. Wiersig, *Rev. Mod. Phys.* **87**, 61 (2015).
- [7] S.-B. Lee, J. Yang, S. Moon, S.-Y. Lee, J.-B. Shim, S. W. Kim, J.-H. Lee, and K. An, *Phys. Rev. Lett.* **103**, 134101 (2009).
- [8] C. Dembowski, H.-D. Gräf, H. L. Harney, A. Heine, W. D. Heiss, H. Rehfeld, and A. Richter, *Phys. Rev. Lett.* **86**, 787 (2001).
- [9] C. Dembowski, B. Dietz, H.-D. Gräf, H. L. Harney, A. Heine, W. D. Heiss, and A. Richter, *Phys. Rev. Lett.* **90**, 034101 (2003).
- [10] A. Kodigala, Th. Lepetit, and B. Kanté, *Phys. Rev. B* **94**, 201103(R) (2016).
- [11] B. Peng, Ş. K. Özdemir, S. Rotter, H. Yilmaz, M. Liertzer, F. Monifi, C. M. Bender, F. Nori, and L. Yang, *Science* **346**, 328 (2014).
- [12] M. Brandstetter, M. Liertzer, C. Deutsch, P. Klang, J. Schöberl, H. E. Türeci, G. Strasser, K. Unterrainer, and S. Rotter, *Nat. Commun.* **5**, 4034 (2014).
- [13] C. E. Rüter, K. G. Makris, R. El-Ganainy, D. N. Christodoulides, M. Segev, and D. Kip, *Nat. Phys.* **6**, 192 (2010).
- [14] A. Guo, G. J. Salamo, D. Duchesne, R. Morandotti, M. Volatier-Ravat, V. Aimez, G. A. Siviloglou, and D. N. Christodoulides, *Phys. Rev. Lett.* **103**, 093902 (2009).
- [15] W. D. Heiss and H. L. Harney, *Eur. Phys. J. D* **17**, 149 (2001).
- [16] B. Peng, Ş. K. Özdemir, M. Liertzer, W. Chen, J. Kramer, H. Yilmaz, J. Wiersig, S. Rotter, and L. Yang, *Proc. Natl. Acad. Sci. U.S.A.* **113**, 6845 (2016).
- [17] P. Miao, Z. Zhang, J. Sun, W. Walasik, S. Longhi, N. M. Litchinitser, and L. Feng, *Science* **353**, 464 (2016).
- [18] H. Deng, H. Haug, and Y. Yamamoto, *Rev. Mod. Phys.* **82**, 1489 (2010).
- [19] I. Carusotto and C. Ciuti, *Rev. Mod. Phys.* **85**, 299 (2013).
- [20] H. Deng, G. Weihs, C. Santori, J. Bloch, and Y. Yamamoto, *Science* **298**, 199 (2002).
- [21] J. Kasprzak, M. Richard, S. Kundermann, A. Baas, P. Jeambrun, J. M. J. Keeling, F. M. Marchetti, M. H. Szymańska, R. André, J. L. Staehli, V. Savona, P. B. Littlewood, B. Deveaud, and L. S. Dang, *Nature (London)* **443**, 409 (2006).
- [22] R. B. Balili, V. Hartwell, D. Snoke, L. Pfeiffer, and K. West, *Science* **316**, 1007 (2007).
- [23] T. Byrnes, N. Y. Kim, and Y. Yamamoto, *Nat. Phys.* **10**, 803 (2014).

- [24] P. G. Savvidis, C. Ciuti, J. J. Baumberg, D. M. Whittaker, M. S. Skolnick, and J. S. Roberts, *Phys. Rev. B* **64**, 075311 (2001).
- [25] L. Zhang, W. Xie, J. Wanga, A. Poddubny, J. Lu, Y. Wang, J. Gu, W. Liu, D. Xu, X. Shen, Y. G. Rubo, B. L. Altshuler, A. V. Kavokin, and Z. Chen, *Proc. Natl. Acad. Sci. U.S.A.* **112**, E1516 (2015).
- [26] F. Baboux, L. Ge, T. Jacqmin, M. Biondi, E. Galopin, A. Lemaître, L. Le Gratiet, I. Sagnes, S. Schmidt, H. E. Türeci, A. Amo, and J. Bloch, *Phys. Rev. Lett.* **116**, 066402 (2016).
- [27] T. Gao, E. Estrecho, K. Y. Bliokh, T. C. H. Liew, M. D. Fraser, S. Brodbeck, M. Kamp, C. Schneider, S. Höfling, Y. Yamamoto, F. Nori, Y. S. Kivshar, A. Truscott, R. Dall, and E. A. Ostrovskaya, *Nature (London)* **526**, 554 (2015).
- [28] E. Wertz, L. Ferrier, D. D. Solnyshkov, R. Johne, D. Sanvitto, A. Lemaître, I. Sagnes, R. Grousson, A. V. Kavokin, P. Senellart, G. Malpuech, and J. Bloch, *Nat. Phys.* **6**, 860 (2010).
- [29] F. Manni, K. G. Lagoudakis, T. C. H. Liew, R. André, and B. Deveaud-Plédran, *Phys. Rev. Lett.* **107**, 106401 (2011).
- [30] P. Cristofolini, A. Dreismann, G. Christmann, G. Franchetti, N. G. Berloff, P. Tsotsis, Z. Hatzopoulos, P. G. Savvidis, and J. J. Baumberg, *Phys. Rev. Lett.* **110**, 186403 (2013).
- [31] A. Askitopoulos, H. Ohadi, A. V. Kavokin, Z. Hatzopoulos, P. G. Savvidis, and P. G. Lagoudakis, *Phys. Rev. B* **88**, 041308(R) (2013).
- [32] G. Tosi, G. Christmann, N. G. Berloff, P. Tsotsis, T. Gao, Z. Hatzopoulos, P. G. Savvidis, and J. J. Baumberg, *Nat. Phys.* **8**, 190 (2012).
- [33] B. Nelsen, G. Liu, M. Steger, D. W. Snoke, R. Balili, K. West, and L. Pfeiffer, *Phys. Rev. X* **3**, 041015 (2013).
- [34] See Supplemental Material <http://link.aps.org/supplemental/10.1103/PhysRevLett.120.065301> for the description of the experimental setup and the measurements, as well as the details on coupled-mode theory and numerical simulations, which includes Refs. [35–41].
- [35] I. V. Basisty, V. Yu. Bazhenov, M. S. Soskin, and M. V. Vasnetsov, *Opt. Commun.* **103**, 422 (1993).
- [36] F. Manni, T. C. H. Liew, K. G. Lagoudakis, C. Ouellet-Plamondon, R. André, V. Savona, and B. Deveaud, *Phys. Rev. B* **88**, 201303(R) (2013).
- [37] S. Khan and H. E. Türeci, *Phys. Rev. A* **94**, 053856 (2016).
- [38] J. Keeling and N. G. Berloff, *Phys. Rev. Lett.* **100**, 250401 (2008).
- [39] M. Wouters, *New J. Phys.* **14**, 075020 (2012).
- [40] M. Wouters, T. C. H. Liew, and V. Savona, *Phys. Rev. B* **82**, 245315 (2010).
- [41] C. Antón, T. C. H. Liew, G. Tosi, M. D. Martín, T. Gao, Z. Hatzopoulos, P. S. Eldridge, P. G. Savvidis, and L. Viña, *Phys. Rev. B* **88**, 035313 (2013).
- [42] M. A. Bandres and J. C. Gutiérrez-Vega, *Opt. Lett.* **29**, 144 (2004).
- [43] The dispersions below condensation threshold can be seen in the Supplemental Material [34].
- [44] W. D. Heiss, *Phys. Rev. E* **61**, 929 (2000).
- [45] M. Wouters and I. Carusotto, *Phys. Rev. Lett.* **99**, 140402 (2007).
- [46] The scaling units are those of length $L = D$, energy $E_0 = \hbar^2/(2m_{\text{ph}}L^2)$, and time $T = \hbar/E_0$, where m_{ph} is the effective mass of the cavity photon. The complex eigenenergy \tilde{E} is normalized by $E_0(1 - |X|^2)$. The normalized real and imaginary parts of the potential are: $V'(\mathbf{r}) = V'_0\Gamma_X P(\mathbf{r})/P_0$, $V''(\mathbf{r}) = V''_0[\Gamma_X P(\mathbf{r})/P_0 - 1]$, where $V'_0 = g_{\text{ex}}\gamma_{\text{ph}}/(E_0R_0)$, $V''_0 = \hbar\gamma_{\text{ph}}/(2E_0)$, and $P_0 = \gamma_R\gamma_{\text{ph}}/R_0$, where γ_{ph} is the lifetime of the cavity photon, g_{ex} is the strength of the exciton-exciton interaction [47], and we have introduced a base value for the stimulated scattering rate R_0 (see Supplemental Material [34]). The dependence on detuning via the Hopfield coefficient is captured by the parameter $\Gamma_X = |X|^2/(1 - |X|^2)$.
- [47] F. Tassone and Y. Yamamoto, *Phys. Rev. B* **59**, 10830 (1999).
- [48] The discrepancy between the experimental linewidth and the imaginary part of the eigenenergy in the effective potential shown in Fig. 5 stems from a somewhat crude approximation of the shape of the non-Hermitian potential in Figs. 4(a) and 4(d). In particular, the width of the right half of the potential is exaggerated in the model to achieve better spectral resolution in simulations. This, in turn, exaggerates the overlap of the modes with the gain region and thus the values of the effective dissipation parameter Γ (see Supplemental Material [34]).
- [49] K. Y. Bliokh, Y. P. Bliokh, V. Freilikher, A. Z. Genack, and P. Sebbah, *Phys. Rev. Lett.* **101**, 133901 (2008).
- [50] A. V. Yulin, A. S. Desyatnikov, and E. A. Ostrovskaya, *Phys. Rev. B* **94**, 134310 (2016).
- [51] G. Nardin, Y. Léger, B. Piętka, F. Morier-Genoud, and B. Deveaud-Plédran, *J. Nanophoton.* **5**, 053517 (2011).
- [52] K. G. Lagoudakis, M. Wouters, M. Richard, A. Baas, I. Carusotto, R. André, Le Si Dang, and B. Deveaud-Plédran, *Nat. Phys.* **4**, 706 (2008).
- [53] G. Roumpos, M. D. Fraser, A. Löffler, S. Höfling, A. Forchel, and Y. Yamamoto, *Nat. Phys.* **7**, 129 (2011).
- [54] D. Sanvitto, F. M. Marchetti, M. H. Szymańska, G. Tosi, M. Baudisch, F. P. Laussy, D. N. Krizhanovskii, M. S. Skolnick, L. Marrucci, A. Lemaître, J. Bloch, C. Tejedor, and L. Vina, *Nat. Phys.* **6**, 527 (2010).
- [55] G. Tosi, G. Christmann, N. G. Berloff, P. Tsotsis, T. Gao, Z. Hatzopoulos, P. G. Savvidis, and J. J. Baumberg, *Nat. Commun.* **3**, 1243 (2012).
- [56] R. Dall, M. D. Fraser, A. S. Desyatnikov, G. Li, S. Brodbeck, M. Kamp, C. Schneider, S. Höfling, and E. A. Ostrovskaya, *Phys. Rev. Lett.* **113**, 200404 (2014).
- [57] M. R. Matthews, B. P. Anderson, P. C. Haljan, D. S. Hall, C. E. Wieman, and E. A. Cornell, *Phys. Rev. Lett.* **83**, 2498 (1999).
- [58] K. W. Madison, F. Chevy, W. Wohlleben, and J. Dalibard, *Phys. Rev. Lett.* **84**, 806 (2000).
- [59] C. Raman, J. R. Abo-Shaer, J. M. Vogels, and W. Ketterle, *Science* **292**, 476 (2001).
- [60] A. E. Leanhardt, A. Görlitz, A. P. Chikkatur, D. Kielpinski, Y. Shin, D. E. Pritchard, and W. Ketterle, *Phys. Rev. Lett.* **89**, 190403 (2002).
- [61] Ch. N. Weiler, T. W. Neely, D. R. Scherer, A. S. Bradley, M. J. Davis, and B. P. Anderson, *Nature (London)* **455**, 948 (2008).
- [62] In atomic condensates, single or multiple vortices are usually created by rotating the confining trap or a “stirring” potential barrier or by direct transfer of orbital angular

- momentum from light to atoms. In polariton condensates, the former is difficult to realize, and the latter works only for resonant excitation schemes [54]. Polariton vortices are reliably generated by employing a nonresonant, multispot excitation with broken cylindrical or chiral symmetry [55,56].
- [63] B. Zhen, C. W. Hsu, Y. Igarashi, L. Lu, I. Kaminer, A. Pick, S.-L. Chua, J. D. Joannopoulos, and M. Soljačić, *Nature (London)* **525**, 354 (2015).
- [64] H. Eleuch and I. Rotter, *Phys. Rev. A* **93**, 042116 (2016).
- [65] J.-W. Ryu, S.-Y. Lee, and S. W. Kim, *Phys. Rev. A* **85**, 042101 (2012).
- [66] W. D. Heiss and G. Wunner, *J. Phys. A* **48**, 345203 (2015).
- [67] H. Jing, Ş. K. Özdemir, H. Lü, and F. Nori, *Sci. Rep.* **7**, 3386 (2017).
- [68] Z. Lin, A. Pick, M. Lončar, and A. W. Rodriguez, *Phys. Rev. Lett.* **117**, 107402 (2016).
- [69] H. Hodaei, A. U. Hassan, S. Wittek, H. Garcia-Gracia, R. El-Ganainy, D. N. Christodoulides, and M. Khajavikhan, *Nature (London)* **548**, 187 (2017).